

## Article

# Automatic 10 m Forest Cover Mapping in 2020 at China's Han River Basin by Fusing ESA Sentinel-1/Sentinel-2 Land Cover and Sentinel-2 near Real-Time Forest Cover Possibility

Xia Wang <sup>1</sup>, Yihang Zhang <sup>2,\*</sup> and Kerong Zhang <sup>1,3,\*</sup>

<sup>1</sup> Key Laboratory of Aquatic Botany and Watershed Ecology, Wuhan Botanical Garden, Chinese Academy of Sciences, Wuhan 430074, China; wangxia@wbgcas.cn

<sup>2</sup> Key Laboratory of Monitoring and Estimate for Environment and Disaster of Hubei Province, Innovation Academy for Precision Measurement Science and Technology, Chinese Academy of Sciences, Wuhan 430071, China

<sup>3</sup> Danjiangkou Wetland Ecosystem Field Scientific Observation and Research Station, The Chinese Academy of Sciences & Hubei Province, Wuhan 430074, China

\* Correspondence: zhangyihang@apm.ac.cn (Y.Z.); kerongzhang@wbgcas.cn (K.Z.)

**Abstract:** Given the increasingly fragmented forest landscapes, it is necessary to map forest cover with fine spatial resolution in a large area. The European Space Agency (ESA) released the 10 m global land cover map in 2020 based on Sentinel-1 and Sentinel-2 images, and Dynamic World provides near real-time possibilities of many land cover classes based on Sentinel-2 images, but they are not designed particularly for forest cover. In this research, we aimed to develop a method to automatically estimate an accurate 10 m forest cover map in 2020 by fusing the ESA forest cover map and Dynamic World near real-time forest cover possibilities. The proposed method includes three main steps: (1) generating stable forest samples, (2) determining the threshold  $T$  and (3) producing the fused forest cover map. China's Han River Basin, dominated by complex subtropical forests, was used as the study site to validate the performance of the proposed method. The results show that the proposed method could produce a forest cover map with the best overall accuracy of  $98.02\% \pm 1.20\%$  and more accurate spatial details compared to using only one of the two data sources. The proposed method is thus superior in mapping forest cover in complex forest landscapes.

**Keywords:** forest cover; Sentinel-2; Sentinel-1; Dynamic World; Han River Basin



**Citation:** Wang, X.; Zhang, Y.; Zhang, K. Automatic 10 m Forest Cover Mapping in 2020 at China's Han River Basin by Fusing ESA Sentinel-1/Sentinel-2 Land Cover and Sentinel-2 near Real-Time Forest Cover Possibility. *Forests* **2023**, *14*, 1133. <https://doi.org/10.3390/f14061133>

Academic Editor: Michael Sprintsin

Received: 5 May 2023

Revised: 28 May 2023

Accepted: 29 May 2023

Published: 30 May 2023



**Copyright:** © 2023 by the authors. Licensee MDPI, Basel, Switzerland. This article is an open access article distributed under the terms and conditions of the Creative Commons Attribution (CC BY) license (<https://creativecommons.org/licenses/by/4.0/>).

## 1. Introduction

Forests are the dominant component of terrestrial ecosystems in terms of the ability to store carbon, regulate climate change and maintain ecosystem functions [1,2], and mapping the spatial distribution dynamics of forest cover with remote sensing is an essential task in environmental science [3–6]. Over the past several decades, various satellite sensor images with spatial resolutions ranging from kilometer to meter scales, such as AVHRR, MODIS, Landsat, Sentinel-2, PALSAR, IKONOS, Quickbird and PlanetScope, have been applied to map forest cover [6–11]. However, given the increasingly fragmented landscapes and inter-annual phenological changes in many forests [12,13], it is necessary to accurately map forest cover with a fine spatial resolution over a large area [14,15].

Satellite sensor images with kilometer- to hundred-meter spatial resolutions, such as AVHRR and MODIS, have an almost daily temporal resolution and are superior in mapping forest cover by tracking the inter-annual phenological changes in different types of forests [8,16,17]. Song et al. [17] quantified the global forest cover changes from 1982 to 2016 based on the generated annual 8 km AVHRR vegetation continuous field (VCF) products. Hansen et al. [8] developed an annual global 250 m VCF product in 2000 based on time-series MODIS images. Both the global AVHRR and MODIS VCF products have been

widely used to estimate forest cover changes at regional and global scales [17–20]. However, due to the coarse spatial resolution, many spatial details of the increasingly fragmented forest cover cannot be accurately observed in AVHRR and MODIS VCF products, and the mixed-pixel issue for forest cover is severe [21]. By contrast, to monitor small-scale forest covers (e.g., individual tree crowns in cities), very fine spatial resolution (VFR) satellite sensor images, such as IKONOS, Quickbird and Worldview, are currently the most critical data sources [22–24]. However, due to the high cost and narrow view width, VFR remote sensing images are rarely used to monitor forest cover and cover changes in a large region. Although 3 m daily PlanetScope four-band images may be a potentially good data source for small-scale forest cover mapping [9], the data access license and massive preprocessing of raw data limit their application in large-area forest cover mapping at present. In general, the cost of VFR satellite sensor images reduces the possibility of carrying out studies at a fine resolution, even more so if using them to address areas of wide spatial extension.

Compared to coarse and very fine spatial resolution remote sensing data, medium spatial resolution satellite sensor images, such as Landsat and Sentinel-2, are currently the most suitable data sources for large-area forest cover mapping [2,25–28] due to the free data access policy, wide view, frequent revisits and ten-meter spatial resolution. It is noteworthy that for the estimation of forest canopy cover, Sentinel-2 performed slightly better than Landsat 8 [26,29]. Moreover, Sentinel-2 images have a finer spatial resolution (e.g., 10 m) and temporal resolution (e.g., 5 days for Sentinel-2A/B since 2018) than those of Landsat images (e.g., 30 m and 16 days revisit frequency), and Sentinel-2 images are superior in large-area forest cover mapping. Besides Sentinel-2 multispectral images, the time-series 10 m Sentinel-1 SAR images also have a comprehensive ability to track canopy changes in forest cover [25,30]. In this regard, the Sentinel-1/2 satellite sensors within the Copernicus program have been a remarkable stride forward by providing high-quality images free of charge with a very acceptable resolution.

Based on both Sentinel-2 and Sentinel-1 data in 2020, the European Space Agency (ESA) initiated the project “WorldCover” to produce a new global baseline land cover map with a 10 m spatial resolution so as to provide valuable land cover information for the environment, earth and climate sciences [31]. The ESA land cover map has a global overall accuracy of 74.4%, while the forest cover has a high accuracy, with a producer’s accuracy of 89.9% and a user’s accuracy of 80.8%, and it thus provides a high-quality 10 m global forest cover map. However, the ESA forest cover map cannot consider the typical features of inter-annual changes in forests, particularly for subtropical mixed forests, and its accuracy is, therefore, limited [32,33]. Fortunately, Dynamic World was developed to provide near real-time possibility maps of nine land cover classes and the highest-probability land cover map by using deep learning and Sentinel-2 images [34]. The time-series forest cover possibilities in Dynamic World data capture the inter-annual phenological changes in various forests, but they are based only on Sentinel-2 images, and the accuracy will be limited by daily frequent clouds and different climatic conditions.

The issue of neglecting inter-annual forest phenological changes in the ESA land cover product can cause confusion between non-evergreen forests and non-forested areas, while the issue of relying solely on Sentinel-2 images as a single data source in the Dynamic World land cover possibility product hampers its ability to provide spatially continuous forest cover. Given that the ESA land cover product and Dynamic World land cover possibility product are not designed particularly for forest cover, an accurate 10 m forest cover map in a large area can hardly be achieved by directly using them. In this research, we aimed to develop a method to automatically estimate an accurate 10 m forest cover map in 2020 by fusing the ESA forest cover map and Dynamic World Sentinel-2 near real-time forest cover possibilities. Firstly, the yearly mean forest cover possibility map was extracted from the near real-time land cover possibilities in Dynamic World. Secondly, the threshold  $T$  was determined for the mean forest cover possibility map based on the collected stable forest samples. Thirdly, the proposed 10 m forest cover map was produced by fusing the ESA forest cover map and mean forest cover possibility map with the help of the threshold

T. China's Han River Basin, dominated by complex landscapes of subtropical forests [35], was used as a typical study site to validate the performance of the proposed method. The proposed method is expected to have a superior ability to map forest cover in complex forest landscapes.

## 2. Materials and Methods

### 2.1. Study Area

The Han River Basin, situated in Central China (see Figure 1a), originates from the Qinling Mountains and flows through Shaanxi and Hubei Provinces before joining the Yangtze River in Wuhan City. The total area of China's Han River Basin is  $\sim 159,000$  km<sup>2</sup>. The Han River Basin falls within the North Subtropical Monsoon Climatic Zone, characterized by an annual mean precipitation of approximately 804 mm and an annual mean temperature ranging from 12 °C to 16 °C. As shown in Figure 1b, forests (e.g., tree cover) are the dominant land cover in the Han River Basin, especially in the western and central mountain areas, in which there are many types of forests: evergreen broadleaf forests, deciduous broadleaf forests, evergreen conifer forests, deciduous conifer forests and mixed forests [35]. In addition, as one of the experimental areas for China's Six Key Forestry and Ecological Programs, the Han River Basin has undergone one of the most significant forest restorations in China and even in the world due to successful forest management and protection policies [17]. As such, accurately mapping forest cover with a fine spatial resolution in the Han River Basin has become a critical task, as it provides up-to-date information on the spatial distribution of forest cover in the region.

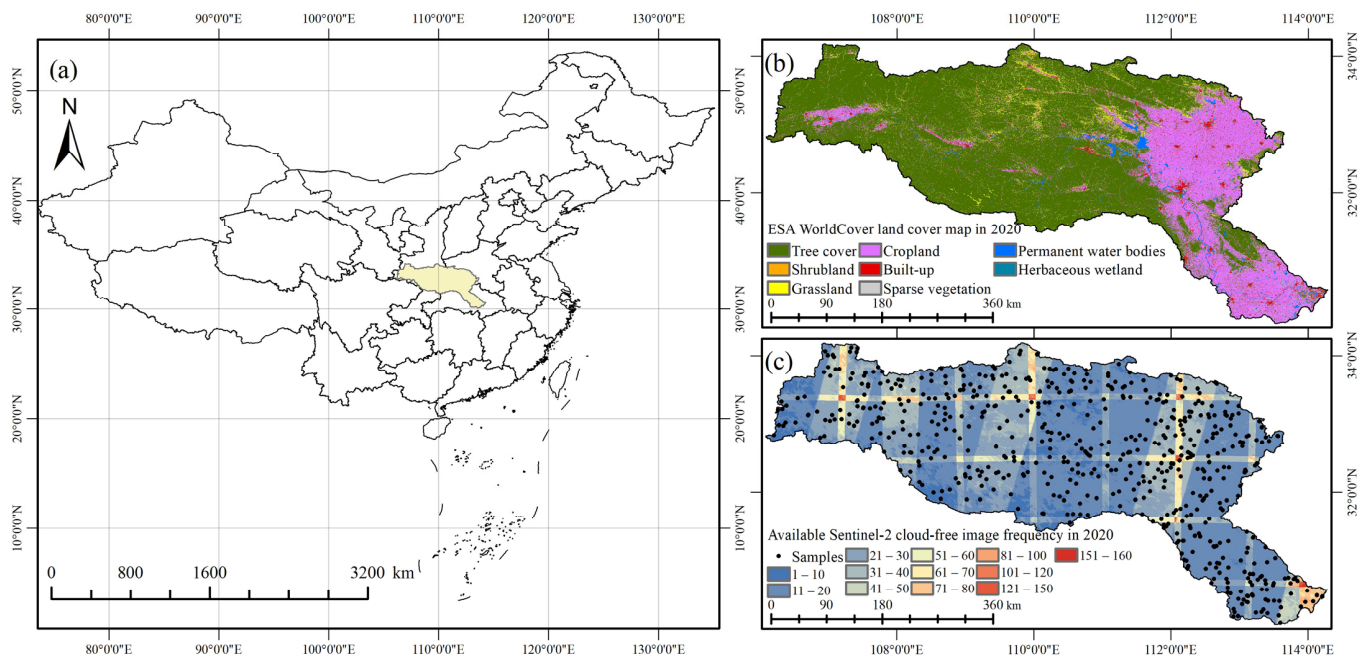


**Figure 1.** Study site and dataset. (a) Geolocation of the Han River Basin in China; (b) ESA WorldCover land cover map in 2020; (c) available Sentinel-2 cloud-free image frequency in the Dynamic World data of 2020 and 600 validation samples.

### 2.2. Data

Two datasets, ESA WorldCover and Dynamic World, are the input data of the proposed method. The ESA WorldCover product is a global land cover map for 2020 with a resolution of 10 m, which was generated using Sentinel-1 and Sentinel-2 data [31]. The original ESA WorldCover product includes 11 land cover classes, but as shown in Figure 1b, there are only 8 land cover classes in the Han River Basin, China, and we focused only on forest cover in this research, in which a forest is defined as tree canopy cover of more than 10%. It

is noteworthy that the products of ESA WorldCover and Dynamic World are ready-to-use datasets, and there is no need to further process the original Sentinel-1 and Sentinel-2 images. Dynamic World is a near real-time global land cover dataset with a 10 m resolution and was generated by utilizing deep learning techniques and Sentinel-2 images that have a cloud percentage of less than 35% [34]. As shown in Figure 1c, the frequency (number) of Sentinel-2 cloud-free images in Dynamic World ranges from place to place in the Han River Basin. Dynamic World also provides class probabilities for nine different land cover classes, and near real-time forest cover possibilities were used in this research. Furthermore, to obtain the samples of stable forest points, annual PALSAR forest/non-forest cover maps for 2017–2020 [10], the annual Global Forest Change map for 2001–2021 [2], the Landsat tree canopy height map for 2020 [36] and the Landsat tree canopy cover map for 2015 [37] were also used as auxiliary datasets. All of the above datasets are freely available on the Google Earth Engine (GEE) platform. Moreover, we collected eight Google Earth images from circa 2020 to provide a photointerpretation for comparing the spatial details of different forest cover maps in Section 3.

### 2.3. Methods

#### 2.3.1. Fused Forest Cover Map Production

Besides the ESA forest cover map and Dynamic World Sentinel-2 near real-time forest cover possibilities in 2020, the proposed method also needs some samples of stable forest points to determine the forest cover segmentation threshold  $T$  for forest cover possibilities in Dynamic World. As shown in Figure 2, the flowchart of the proposed method is composed of the following three sections: (1) generating stable forest samples, (2) determining the threshold  $T$  and (3) producing the fused forest cover map.

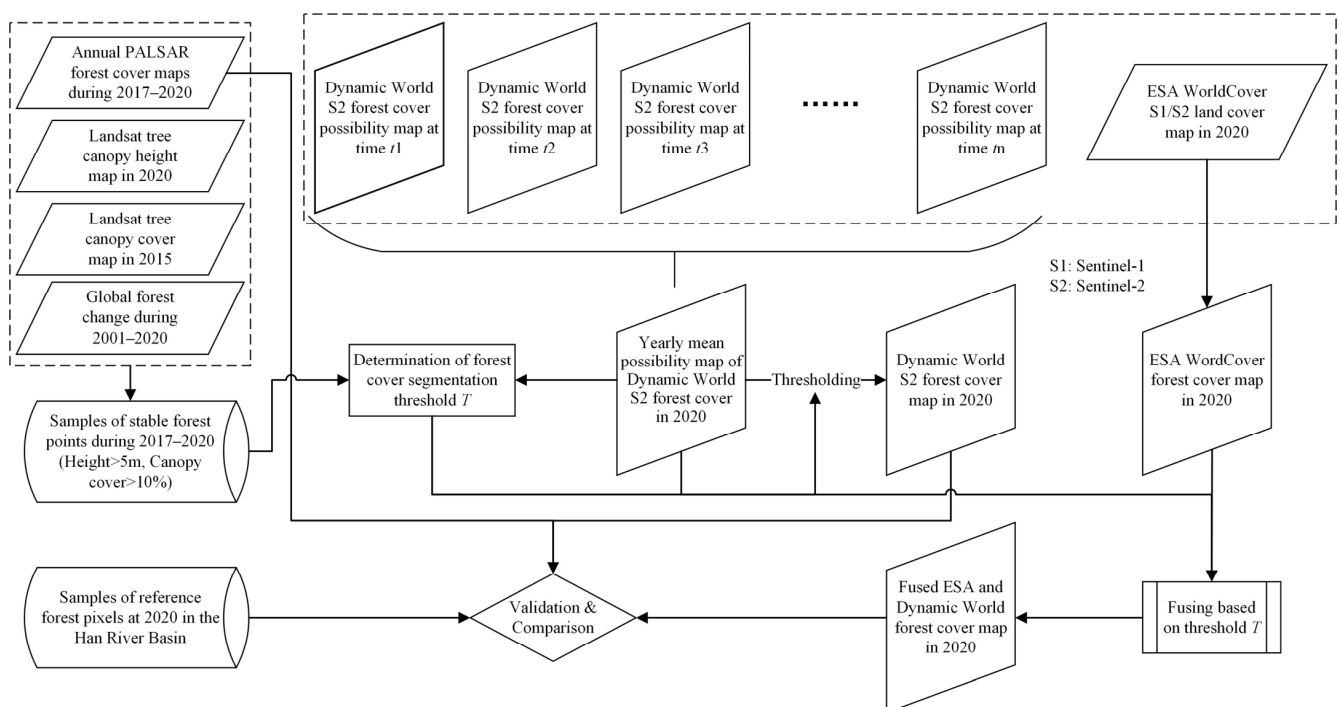


**Figure 2.** Flowchart of the proposed method.

Stable forest samples refer to forest cover pixels that experienced no significant changes (e.g., loss) during a period, and they are used to determine the forest cover segmentation threshold  $T$  for forest cover possibilities in Dynamic World. Four auxiliary datasets, namely, the annual PALSAR forest cover maps for 2017–2020 [10], the annual Global Forest Change map for 2001–2021 [2], the Landsat tree canopy height map for 2020 [36] and the Landsat tree canopy cover map for 2015 [37], were used here to collect the stable forest samples.

Stable forests were initially identified by comparing consistent forests across the 2017, 2018, 2019 and 2020 PALSAR forest cover maps. Meanwhile, any forest-loss pixels in the Global Forest Change map were excluded from the stable forests, and forest height less than 5 m and canopy cover less than 10% were also excluded by using the tree canopy height map and canopy cover map, respectively. Finally, 1007 samples of stable forests were randomly selected. With the stable forest samples and a forest cover possibility map, the mean and standard deviation values of forest cover possibilities for 1007 samples can be calculated, and then the forest cover segmentation threshold can be predicted from the difference between the mean and standard deviation values; more information about this can be found in Equation (1) below.

Near real-time forest cover possibility maps in the Dynamic World data record inter-annual changes in various forests, but they were extracted from Sentinel-2 images, and the spatial consistency was seriously impacted by frequent clouds and shadows. We, therefore, used the yearly mean forest cover possibility map based on all available forest cover possibility maps in 2020. Assuming that the mean yearly mean forest cover possibility map is  $FP$ , the threshold  $T$  used to segment  $FP$  into a forest cover map by using the stable forest samples can be expressed as [38,39]:

$$T = FP_{\text{mean}}(\text{stable}) - 1.96 \times FP_{\text{std}}(\text{stable}), \quad (1)$$

in which  $T$  represents the threshold value in year  $y$ .  $FP_{\text{mean}}(\text{stable})$  and  $FP_{\text{std}}(\text{stable})$  represent the mean and standard deviation, respectively, of the yearly mean forest cover possibility map values for stable forest samples in that year. With the threshold  $T$ , a forest cover map can be generated from the yearly mean forest cover possibility map.

With the ESA forest cover binary map and Dynamic World yearly mean forest cover possibility map, we aimed to produce a fused forest cover map by using the above threshold  $T$ . Assuming that the ESA forest cover binary map is  $FC_{\text{ESA}}$  and the fused forest cover binary map is  $FC_{\text{fuse}}$ , the fusing process can be expressed as:

$$FC_{\text{fuse}}(i) = \begin{cases} FC_{\text{ESA}}(i), & \text{if } 0.5T < FP_{\text{mean}}(i) < 1.5T \\ 1, & \text{if } FP_{\text{mean}}(i) \geq 1.5T \\ 0, & \text{if } FP_{\text{mean}}(i) \leq 0.5T \end{cases} \quad (2)$$

Equation (2) means that for a pixel  $i$  in the fused forest cover binary map, if the forest cover possibility value of  $FP_{\text{mean}}(i)$  is larger than  $1.5T$  or less than  $0.5T$ , it will be regarded as a forest pixel or non-forest pixel, respectively. Otherwise, it will be equal to the ESA forest cover map, the binary value of  $FC_{\text{ESA}}(i)$ .

### 2.3.2. Accuracy Assessment

To perform a comprehensive validation of the performance of the fused forest cover map in 2020, we used the above forest cover map generated by using the threshold  $T$ , along with the ESA forest cover map [31] and the PALSAR forest cover map [10] for comparisons. For accuracy validation, the overall accuracy, producer's accuracy and user's accuracy were calculated for different forest cover maps. To obtain an unbiased statistical estimation of the accuracy of the three forest cover maps when the strata are different from the map classes, we employed the method described by Stehman et al. [40,41] to estimate the overall accuracy, producer's accuracy and user's accuracy and the corresponding 1.96 standard errors with a 95% confidence interval.

As shown in Figure 1c, 600 reference sample points were collected using stratified random sampling, with the forest and non-forest classes each having 300 sample points. Specifically, the 600 validation sample points for forest and non-forest classes were first extracted from the 10 m forest cover map produced by the proposed method, and then very fine spatial resolution Google Earth images were used to determine the forest cover class of each sample point by visual interpretation. It is noteworthy that there is no relationship between the 600 reference sample points and the above 1007 stable forest samples. Because

the PALSAR forest cover map has a spatial resolution of 25 m, it was down-sampled to 10 m with a nearest-neighbor interpolation method so as to have the same spatial resolution as the ESA forest cover map and fused forest cover map.

### 3. Results

#### 3.1. Fused Forest Cover Map Production and Comparison

Due to the significant impact of frequent cloud cover in the study site, the available Sentinel-2 cloud-free images in the Dynamic World data for 2020 were limited to a range of 11–20 for most regions, with the exception of some overlapping regions, as illustrated in Figure 1c. In particular, Figure 3 illustrates the near real-time inter-annual dynamics of forest cover possibilities for four typical stable forest pixels with different available numbers of Sentinel-2 images in the Dynamic World data. Although the four forest pixels have different numbers of observation data, most of their valid observation data are lacking from June to October, which may be related to the fact that the rainy season of the Han River Basin is in these months. All four typical forest pixels present similar phenological dynamics and curve fitting, which have low possibility values in the cold months and high values in the warm months from April to September.

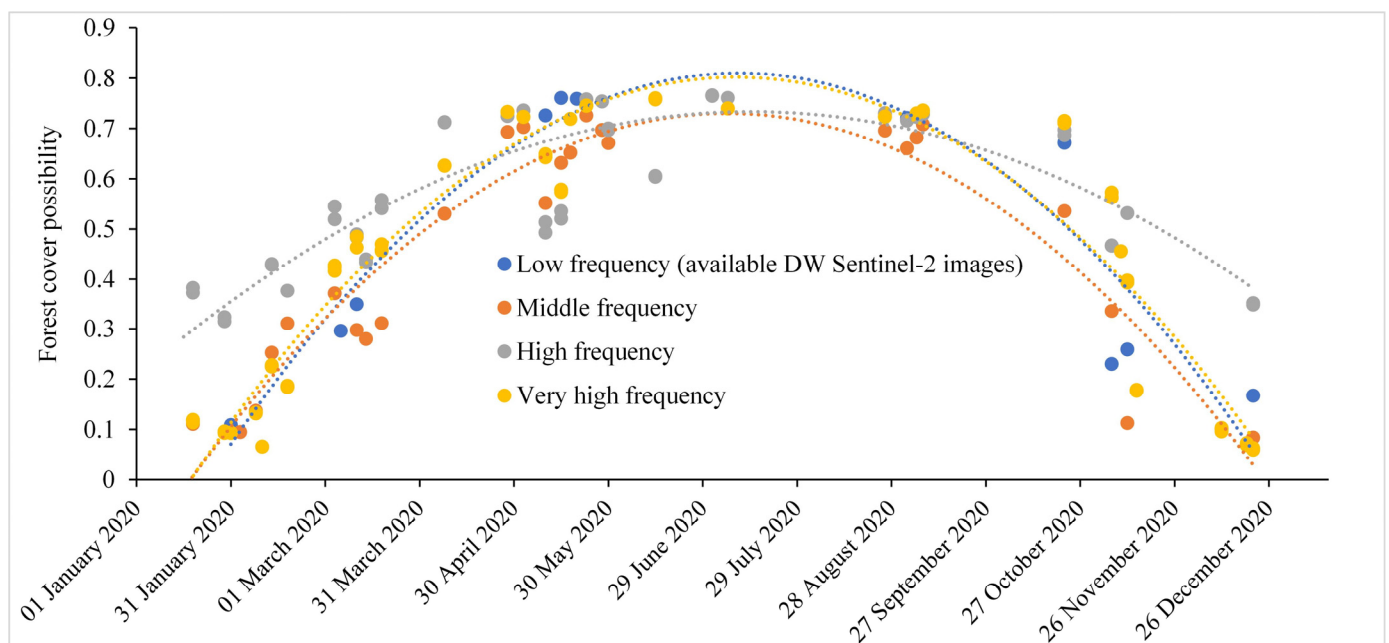


**Figure 3.** Daily dynamics of forest cover possibilities for four stable forest pixels with different available Sentinel-2 image frequencies in the Dynamic World dataset.

To provide a clear illustration of the spatiotemporal dynamics of forest cover possibilities in the Dynamic World data, Figure 4 shows the monthly mean forest cover possibility maps in the Han River Basin based on all near real-time Sentinel-2 data. Besides May and October 2020, the remaining ten months had missing data to some extent, particularly for January, July and December. For the change in forest cover possibilities, relatively low values were observed from January to March and from November to December, while the values from April to October (spring and summer) remained higher; this matches well with the inter-annual phenological changes in vegetation. For the cropland area (Figure 1b) in the eastern part of the Han River Basin, the forest cover possibility values were relatively high in cold months, particularly in February, but they were close to zero in many months (e.g., May); this may be caused by the growth of winter wheat. Nevertheless, certain forest-covered areas, such as those in the southeastern Han River Basin, still exhibit slightly higher probability values compared to others, even during colder months, such as January to March and November to December. This may be because there are many types

of forests, including evergreen broadleaf forests, deciduous broadleaf forests, evergreen conifer forests, deciduous conifer forests and mixed forests, in the Han River Basin, China. Thus, it is difficult to rely on a forest cover probability map during a particular month or short period to distinguish forest cover in the Han River Basin.

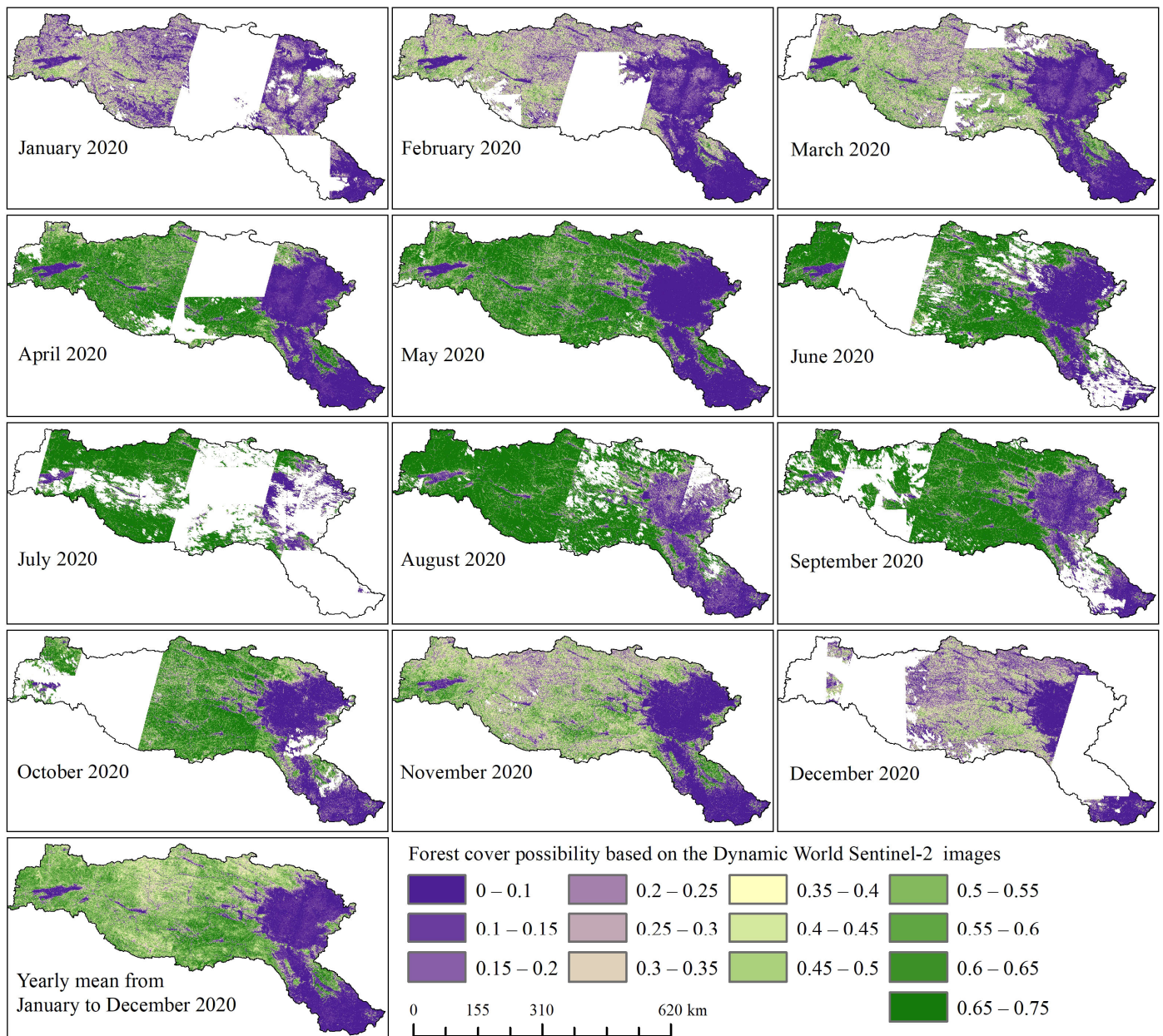


**Figure 4.** Monthly and yearly mean forest cover possibility maps in the Han River Basin based on Sentinel-2 near real-time Dynamic World data in 2020.

By averaging all near real-time forest cover possibility maps, we obtained the yearly mean forest cover possibility map shown in Figure 4, which shows that there are no missing data in the above monthly possibility maps. Compared with the land cover map in Figure 1b, the spatial distribution of yearly mean forest cover possibilities matches well with the ESA tree cover in 2020. Besides the forest cover map produced by the proposed method, the forest cover map generated from the yearly mean forest cover possibility map by using the threshold  $T$ , the ESA forest cover map and the PALSAR forest cover map were also used for a comparison, as shown in Figure 5. Given the yearly mean forest

cover possibility map, the threshold  $T$  was calculated as 0.34 with Equation (1), which was used to convert the possibility map into the 10 m forest cover map shown in Figure 5c. Meanwhile, with inputs of the ESA forest cover map (Figure 5b), the Dynamic World forest cover possibility map (Figure 4) and the threshold  $T$  (0.34), we produced the fused 10 m forest cover map shown in Figure 5d by using Equation (2). For the PALSAR forest cover map shown in Figure 5a, the original two classes of dense forest and non-dense forest were both regarded as forest cover.

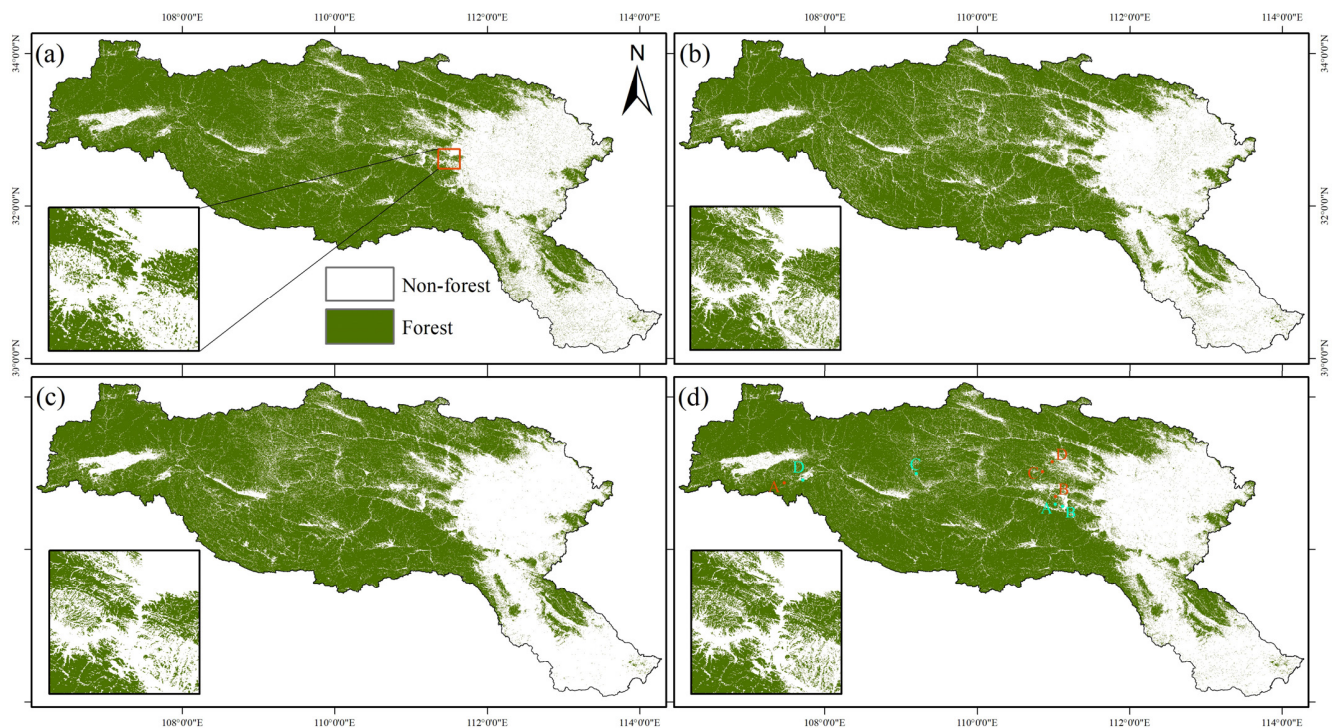


**Figure 5.** Forest cover maps in 2020 for different products and methods. (a) The 25 m forest cover map based on the ALOS-2 PALSAR-2 forest/non-forest product; (b) the 10 m forest cover map extracted from the ESA land cover map; (c) the 10 m forest cover map generated from the Dynamic World yearly mean forest cover possibility map; (d) the 10 m forest cover map generated by fusing ESA forest cover and Dynamic World yearly mean forest cover possibility maps, in which cyan A–D and orange A–D indicate the locations of zoomed areas in Figures 6 and 7, respectively.

Upon comparing the four forest cover maps shown in Figure 5a–d, a similar trend can be observed in the spatial distribution of forest cover among them, especially in dense forest areas, but they have different spatial details. The 10 m forest cover map shown in Figure 5c, generated from the Dynamic World yearly mean forest cover possibility map, has comparatively less forest cover in the eastern part of the Han River Basin. This could be attributed to the elimination of many small-scale forests that had probability values below the threshold  $T$ . For the zoomed areas near Danjiangkou Reservoir in Figure 5, it can also be found that the ESA forest cover map (Figure 5b) and the fused forest cover map (Figure 5d) have more forests than the Dynamic World forest cover map (Figure 5c) and PALSAR forest cover map (Figure 5a) in non-dense forest areas.

For a more detailed comparison of spatial details, we present zoomed-in areas of the four forest cover maps in Figures 6 and 7, with Figure 6 highlighting commission errors and Figure 7 emphasizing omission errors. Due to the lower spatial resolution of 25 m, the PALSAR forest cover map tends to miss small-scale forests (e.g., zoomed areas A and B in Figure 6), but it can also overestimate forest cover in some instances (e.g., zoomed areas C and D in Figure 6). The four zoomed areas of the ESA forest cover map exhibit some overestimation of forest cover in built-up areas. The Dynamic World forest cover

map exhibits over-smoothed forest cover boundaries, which can be attributed to the deep learning method used to produce land cover probabilities having a strong denoising ability. Although this approach has a low commission error, it tends to miss small-scale forests. Our proposed results not only capture many spatial details missed by the Dynamic World forest cover map but also eliminate overestimated forests in the ESA forest cover map. Furthermore, the proposed results exhibit the highest similarity to the forests in VFR satellite images.

A similar trend to that observed in Figure 6 can also be seen in Figure 7, particularly for the PALSAR and Dynamic World forest cover maps. The four zoomed areas of the ESA forest cover map exhibit some underestimation of forest cover, especially for zoomed areas C and D. By contrast, the proposed method can not only detect many missed forests in the Dynamic World forest cover map but also eliminate some commission errors in the Dynamic World results. Meanwhile, many missed forests in the ESA forest cover map were also well-maintained by the results of the proposed method. This is because our proposed method combines the advantages of both the ESA forest cover map and the Dynamic World forest cover possibility map while reducing their uncertainties to some extent.

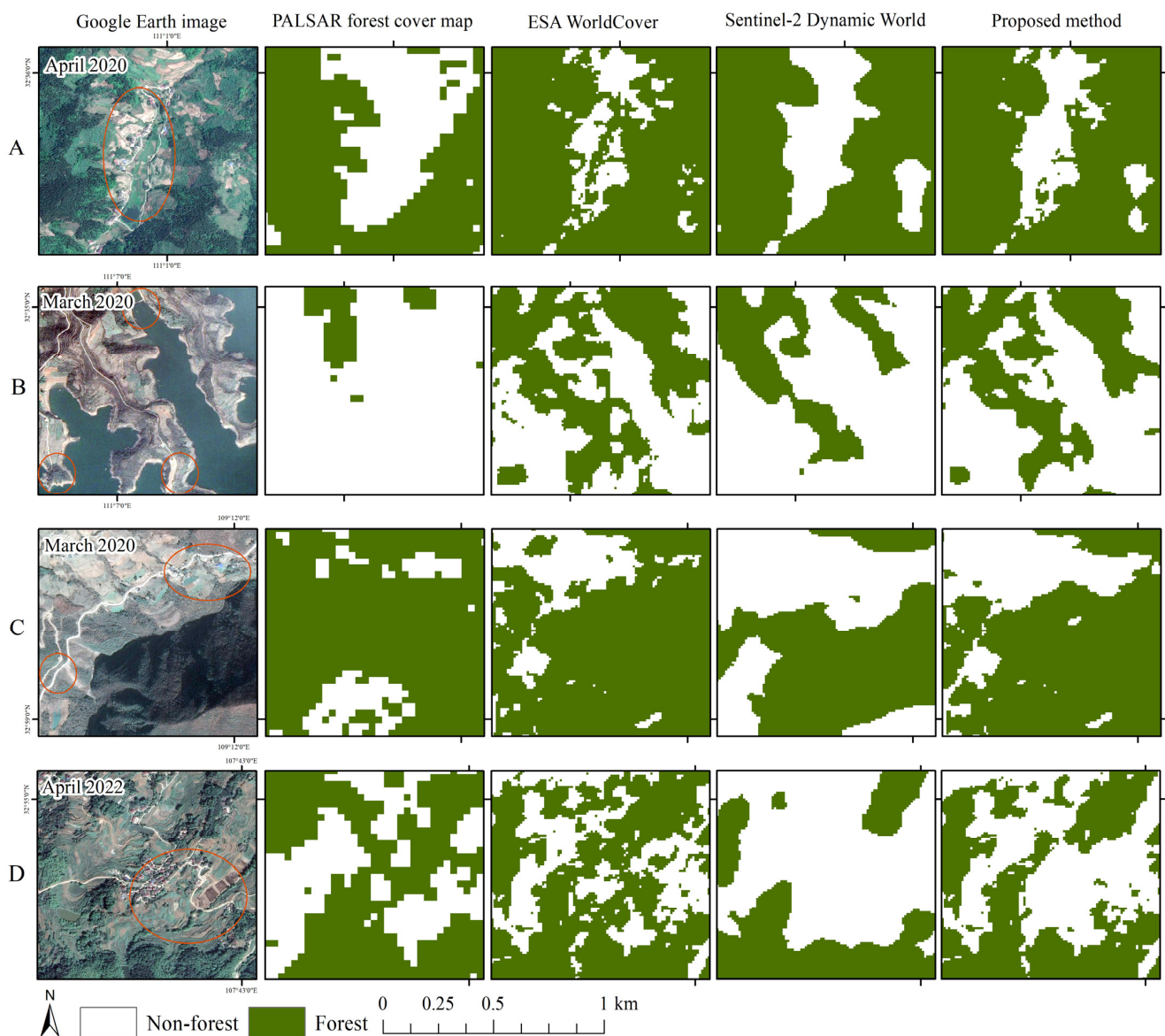


**Figure 6.** Google Earth images and corresponding zoomed areas of four forest cover maps produced by different products and methods, and their locations are shown in Figure 5d (cyan A–D labels).

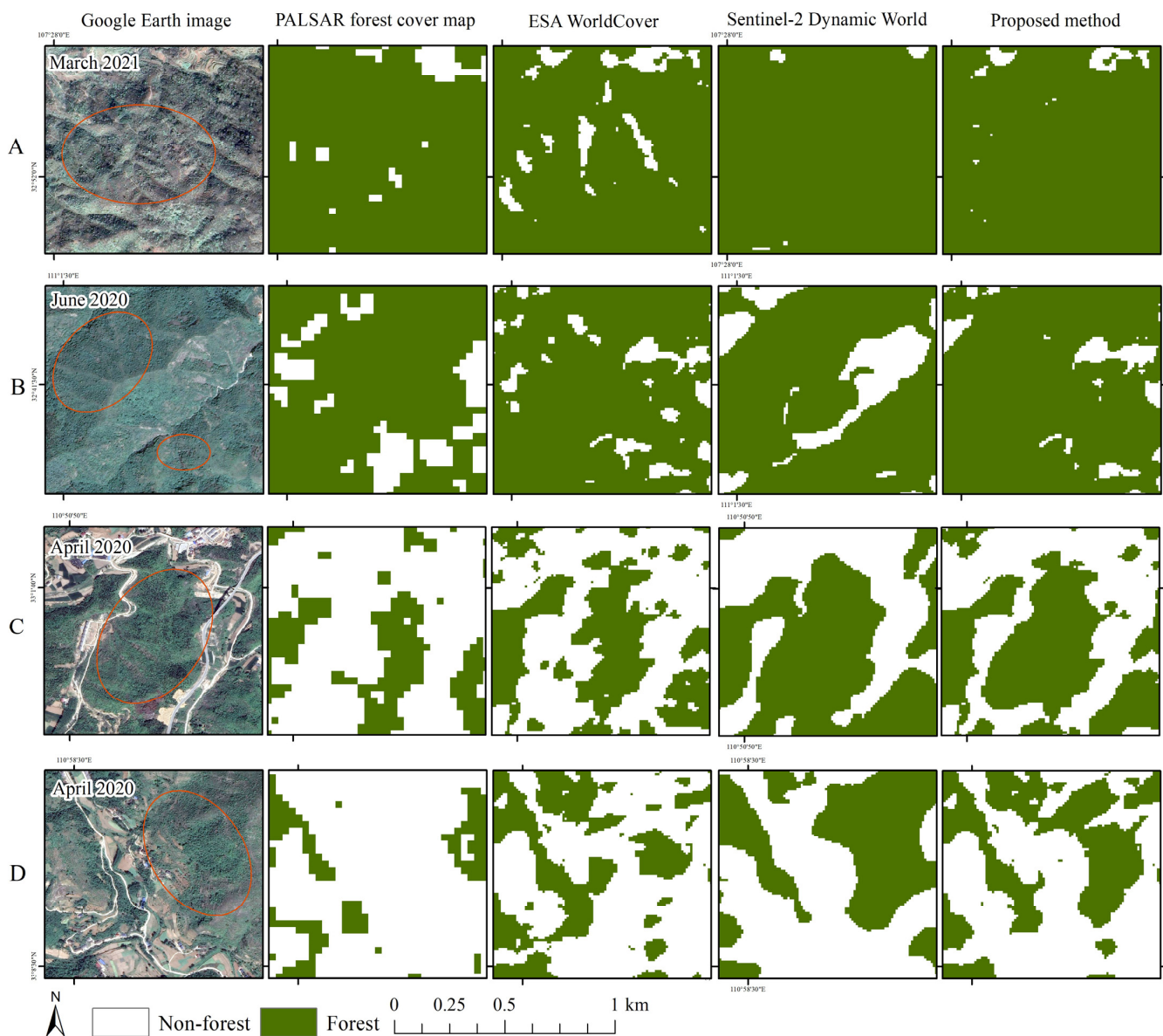


**Figure 7.** Google Earth images and corresponding zoomed areas of four forest cover maps produced by different products and methods, and their locations are shown in Figure 5d (orange A–D labels).

### 3.2. Accuracy Assessment

The accuracy assessment presented in Table 1 also indicates that the PALSAR forest cover map has the worst accuracy, with the smallest overall accuracy of  $89.29\% \pm 2.55\%$  and producer's and user's accuracy values of  $90.63\% \pm 3.29\%$  and  $92.34\% \pm 2.31\%$  for forest cover, respectively. The accuracies of ESA and Dynamic World forest cover maps both have notable improvements over the PALSAR forest cover map. Although the ESA forest cover map has a higher producer's accuracy than the Dynamic World forest cover map, its user's accuracy is slightly smaller. The proposed forest cover map outperforms the other maps in terms of both the best overall accuracy of  $98.02\% \pm 1.20\%$  and the best producer's and user's accuracies of  $99.25\% \pm 0.72\%$  and  $97.67\% \pm 1.71\%$ , respectively, indicating its superiority in mapping forest cover in the complex forest landscapes of the Han River Basin, China.

**Table 1.** Accuracy assessment of different forest cover maps.

Forest Cover Maps	Overall Accuracy *	Producer's Accuracy *		User's Accuracy *	
		Forest	Non-Forest	Forest	Non-Forest
PALSAR	89.29% ± 2.55%	90.63% ± 3.29%	86.96% ± 3.99%	92.34% ± 2.31%	84.25% ± 4.76%
ESA	96.74% ± 1.43%	98.91% ± 0.98%	92.97% ± 3.38%	96.07% ± 1.97%	98.01% ± 1.79%
Dynamic World	95.33% ± 1.76%	96.24% ± 2.13%	93.76% ± 3.05%	96.4% ± 1.79%	93.49% ± 3.47%
Proposed	98.02% ± 1.20%	99.25% ± 0.72%	95.89% ± 2.89%	97.67% ± 1.71%	98.67% ± 1.30%

\* “±” means 1.96 standard error with a 95% confidence interval.

#### 4. Discussion

Based on the visual comparison and statistical accuracy assessment conducted above, it is evident that the proposed method outperforms the PALSAR, ESA and Dynamic World forest cover maps in terms of producing a 10 m forest cover map with reduced commission and omission errors. This is particularly notable for the large expansive area of the Han River Basin in China. Although the fused forest cover map was generated by combining the ESA forest cover map and the Dynamic World yearly mean forest cover possibility map, the proposed result offers superior spatial details compared to relying solely on either of the two data sources. Moreover, it is noteworthy that the products of ESA World Cover and Dynamic World are ready-to-use datasets, and there is no need for the proposed method to further process the original Sentinel-1 and Sentinel-2 images. While both the ESA forest cover map and the Dynamic World yearly mean forest cover possibility map have their own strengths and weaknesses in representing multi-scale forest patches, the fused forest cover map successfully inherits the advantages and mitigates the disadvantages of both, aligning with the original intention behind the proposed method.

The ESA forest cover map was produced based on Sentinel-1 and Sentinel-2 images in 2020, and it can, thus, take advantage of Sentinel-1 SAR and Sentinel-2 multispectral data in the mapping process [31,42]. For example, the C-band SAR of Sentinel-1 images has the ability to penetrate clouds and obtain the tree canopy structure information, which will provide complementary information for Sentinel-2 images in forest cover mapping so as to finally improve the accuracy [43,44]. The above results prove this key point, as the ESA forest cover map could have better performance in presenting many spatial details of forests than the PALSAR and Dynamic World forest cover maps. In contrast, the use of Sentinel-1 SAR images in the ESA forest cover map may introduce some uncertainties, including the omission of numerous forests, but they can be readily identified using multispectral images from Sentinel-2, as evident in the zoomed areas in Figure 7. More importantly, it should be noted that the ESA forest cover map is unable to account for inter-annual phenological variations in many forest types, such as the dominant deciduous broadleaf forest, deciduous conifer forest and mixed forest in the Han River Basin, China [35]. This is significant because these forest types demonstrate distinct forest cover possibility values in different seasons, which will also lead to many commission and omission errors in the ESA forest cover map, as shown in Figures 6 and 7.

The near real-time forest cover possibilities from the Dynamic World data can capture the time-series phenological changes in various forest types, as evident in Figures 3 and 4. Given the inter-annual phenological changes in various forests and the frequent occurrence of clouds in the Han River Basin, mapping forest cover using Dynamic World possibility data within a short period can be challenging. The yearly mean possibility based on the near real-time Dynamic World data is a solution to provide spatially consistent information for forest cover mapping. As shown in the above results, although the forest cover map extracted from the yearly mean possibility in Dynamic World data effectively represented most of the forests, the boundaries of many forests were over-smoothed, and the omission error was high. It is, therefore, necessary to fuse the ESA forest cover map and the Dynamic World forest cover possibility map so as to produce a more accurate 10 m forest cover map of the Han River Basin, China.

In the mean forest cover possibility map shown in Figure 4, some forests may still have small mean possibility values, such as less than 0.5  $T$ ; this may be caused by the extremely few available cloud-free Dynamic World Sentinel-2 images. In this way, the real forest cover may be regarded as non-forest cover, and this is one source of uncertainty for the proposed method. In fact, the dynamics of near real-time forest cover possibilities shown in Figure 3 are similar to the phenological changes observed by using the NDVI index [4,45]. In future work, it would be of great interest to explore the use of spatiotemporal filtering techniques, such as the Savitzky–Golay filter [46], to reconstruct high-quality time-series forest cover possibility data. Moreover, using spatiotemporal fusion techniques, such as the spatial and temporal adaptive reflectance fusion model (STARFM) [47], enhanced STARFM [48] and enhanced Flexible Spatiotemporal DATA Fusion (SFSDAF) [49], can also help to reconstruct high-quality 10 m forest cover possibility data. This would help to reduce the uncertainty caused by frequent missing cloud-free Sentinel-2 data due to frequent cloud cover in the Han River Basin.

## 5. Conclusions

Given the increasingly fragmented landscapes of various forest types, including evergreen broadleaf forests, deciduous broadleaf forests, evergreen conifer forests, deciduous conifer forests and mixed forests, in China's Han River Basin, it is a challenging but essential task to produce an accurate fine spatial resolution forest cover map. The ESA forest cover map based on Sentinel-1 and Sentinel-2 images does make use of the advantages of both Sentinel-1 SAR and Sentinel-2 multispectral data. However, it is still plagued by many commission and omission errors, as it is unable to account for inter-annual phenological variations in many forest types. Fortunately, Dynamic World was developed to provide near real-time possibility maps of forest cover using deep learning and Sentinel-2 images. However, the generated forest cover map often suffers from over-smoothed boundaries and may miss many small-scale forests.

In this research, we proposed a method to combine the advantages of both the ESA forest cover map and the Dynamic World forest cover possibility map while reducing their uncertainties to some extent. The results showed that our proposed method not only captured many spatial details missed by the Dynamic World forest cover map but also eliminated many overestimated forests in the ESA forest cover map, and it produced a forest cover map with the best overall accuracy of  $98.02\% \pm 1.20\%$  when compared with the ESA, Dynamic World and the PALSAR forest cover maps. The fused forest cover map successfully inherits the advantages and mitigates the disadvantages of the ESA and Dynamic World forest cover maps, aligning with the original intention behind the proposed method. The proposed method is, therefore, superior in mapping forest cover in the complex forest landscapes of the Han River Basin, China. However, frequent clouds seriously impact the near real-time forest cover possibilities in the Dynamic World data, which will cause outliers in the final fused forest cover map. In future work, it would be of high interest to apply spatiotemporal filtering techniques, such as the Savitzky–Golay filter, to reconstruct high-quality time-series Dynamic World forest cover possibility maps so as to increase the accuracy of the fused forest cover map.

**Author Contributions:** Experimentation, data analysis, visualization and writing—original draft preparation, X.W.; conceptualization, methodology, validation and writing—review and editing, supervision, Y.Z.; conceptualization, writing—review and editing and supervision, K.Z.; funding acquisition, K.Z., Y.Z. and X.W. All authors have read and agreed to the published version of the manuscript.

**Funding:** This research was funded by the National Natural Science Foundation of China (42271400, 31922060), the Hubei Provincial Natural Science Foundation of China (2020CFB233), the Key Research Program of Frontier Sciences, Chinese Academy of Sciences (ZDBS-LY-DQC034), the Hubei Provincial Natural Science Foundation of China for Distinguished Young Scholars (2022CFA045) and the Yellow Crane Talent Program of Wuhan.

**Data Availability Statement:** The 2020 forest cover map of China’s Han River Basin at a spatial resolution of 10 m is available at <https://doi.org/10.5281/zenodo.7980298> (accessed on 4 May 2023).

**Conflicts of Interest:** The authors declare no conflict of interest.

## References

- Harris, N.L.; Gibbs, D.A.; Baccini, A.; Birdsey, R.A.; de Bruin, S.; Farina, M.; Fatoyinbo, L.; Hansen, M.C.; Herold, M.; Houghton, R.A.; et al. Global maps of twenty-first century forest carbon fluxes. *Nat. Clim. Chang.* **2021**, *11*, 234–240. [[CrossRef](#)]
- Hansen, M.C.; Potapov, P.V.; Moore, R.; Hancher, M.; Turubanova, S.A.; Tyukavina, A.; Thau, D.; Stehman, S.V.; Goetz, S.J.; Loveland, T.R.; et al. High-Resolution Global Maps of 21st-Century Forest Cover Change. *Science* **2013**, *342*, 850–853. [[CrossRef](#)]
- Hansen, M.C.; Stehman, S.V.; Potapov, P.V. Quantification of global gross forest cover loss. *Proc. Natl. Acad. Sci. USA* **2010**, *107*, 8650–8655. [[CrossRef](#)] [[PubMed](#)]
- Zhang, Y.; Ling, F.; Foody, G.M.; Ge, Y.; Boyd, D.S.; Li, X.; Du, Y.; Atkinson, P.M. Mapping annual forest cover by fusing PALSAR/PALSAR-2 and MODIS NDVI during 2007–2016. *Remote Sens. Environ.* **2019**, *224*, 74–91. [[CrossRef](#)]
- Qin, Y.; Xiao, X.; Dong, J.; Zhang, Y.; Wu, X.; Shimabukuro, Y.; Arai, E.; Biradar, C.; Wang, J.; Zou, Z.; et al. Improved estimates of forest cover and loss in the Brazilian Amazon in 2000–2017. *Nat. Sustain.* **2019**, *2*, 764–772. [[CrossRef](#)]
- Dong, J.; Xiao, X.; Sheldon, S.; Biradar, C.; Duong, N.D.; Hazarika, M. A comparison of forest cover maps in Mainland Southeast Asia from multiple sources: PALSAR, MERIS, MODIS and FRA. *Remote Sens. Environ.* **2012**, *127*, 60–73. [[CrossRef](#)]
- Lui, G.V.; Coomes, D.A. A Comparison of Novel Optical Remote Sensing-Based Technologies for Forest-Cover/Change Monitoring. *Remote Sens.* **2015**, *7*, 2781–2807. [[CrossRef](#)]
- Hansen, M.C.; DeFries, R.S.; Townshend, J.R.G.; Sohlberg, R.; Dimiceli, C.; Carroll, M. Towards an operational MODIS continuous field of percent tree cover algorithm: Examples using AVHRR and MODIS data. *Remote Sens. Environ.* **2002**, *83*, 303–319. [[CrossRef](#)]
- Francini, S.; McRoberts, R.E.; Giannetti, F.; Mencucci, M.; Marchetti, M.; Scarascia Mugnozza, G.; Chirici, G. Near-real time forest change detection using PlanetScope imagery. *Eur. J. Remote Sens.* **2020**, *53*, 233–244. [[CrossRef](#)]
- Shimada, M.; Itoh, T.; Motooka, T.; Watanabe, M.; Shiraiishi, T.; Thapa, R.; Lucas, R. New global forest/non-forest maps from ALOS PALSAR data (2007–2010). *Remote Sens. Environ.* **2014**, *155*, 13–31. [[CrossRef](#)]
- Ren, C.; Chen, L.; Wang, Z.; Zhang, B.; Xi, Y.; Lu, C. Spatio-Temporal Changes of Forests in Northeast China: Insights from Landsat Images and Geospatial Analysis. *Forests* **2019**, *10*, 937. [[CrossRef](#)]
- Hansen Matthew, C.; Wang, L.; Song, X.-P.; Tyukavina, A.; Turubanova, S.; Potapov Peter, V.; Stehman Stephen, V. The fate of tropical forest fragments. *Sci. Adv.* **2020**, *6*, eaax8574. [[CrossRef](#)] [[PubMed](#)]
- Gray, R.E.J.; Ewers, R.M. Monitoring Forest Phenology in a Changing World. *Forests* **2021**, *12*, 297. [[CrossRef](#)]
- Zhang, Y.; Li, X.; Ling, F.; Atkinson, P.M.; Ge, Y.; Shi, L.; Du, Y. Updating Landsat-based forest cover maps with MODIS images using multiscale spectral-spatial-temporal superresolution mapping. *Int. J. Appl. Earth Obs. Geoinf.* **2017**, *63*, 129–142. [[CrossRef](#)]
- Li, X.; Ling, F.; Foody, G.M.; Ge, Y.; Zhang, Y.; Du, Y. Generating a series of fine spatial and temporal resolution land cover maps by fusing coarse spatial resolution remotely sensed images and fine spatial resolution land cover maps. *Remote Sens. Environ.* **2017**, *196*, 293–311. [[CrossRef](#)]
- Achard, F.; Estreguil, C. Forest classification of Southeast Asia using NOAA AVHRR data. *Remote Sens. Environ.* **1995**, *54*, 198–208. [[CrossRef](#)]
- Song, X.-P.; Hansen, M.C.; Stehman, S.V.; Potapov, P.V.; Tyukavina, A.; Vermote, E.F.; Townshend, J.R. Global land change from 1982 to 2016. *Nature* **2018**, *560*, 639–643. [[CrossRef](#)] [[PubMed](#)]
- Gao, Y.; Ghilardi, A.; Mas, J.-F.; Quevedo, A.; Paneque-Gálvez, J.; Skutsch, M. Assessing forest cover change in Mexico from annual MODIS VCF data (2000–2010). *Int. J. Remote Sens.* **2018**, *39*, 7901–7918. [[CrossRef](#)]
- Chen, H.; Zeng, Z.; Wu, J.; Peng, L.; Lakshmi, V.; Yang, H.; Liu, J. Large Uncertainty on Forest Area Change in the Early 21st Century among Widely Used Global Land Cover Datasets. *Remote Sens.* **2020**, *12*, 3502. [[CrossRef](#)]
- Song, X.-P.; Huang, C.; Sexton, J.O.; Channan, S.; Townshend, J.R. Annual Detection of Forest Cover Loss Using Time Series Satellite Measurements of Percent Tree Cover. *Remote Sens.* **2014**, *6*, 8878–8903. [[CrossRef](#)]
- Zhang, Y.; Foody, G.M.; Ling, F.; Li, X.; Ge, Y.; Du, Y.; Atkinson, P.M. Spatial-temporal fraction map fusion with multi-scale remotely sensed images. *Remote Sens. Environ.* **2018**, *213*, 162–181. [[CrossRef](#)]
- Goetz, S.J.; Wright, R.K.; Smith, A.J.; Zinecker, E.; Schaub, E. IKONOS imagery for resource management: Tree cover, impervious surfaces, and riparian buffer analyses in the mid-Atlantic region. *Remote Sens. Environ.* **2003**, *88*, 195–208. [[CrossRef](#)]
- Johansen, K.; Coops, N.C.; Gergel, S.E.; Stange, Y. Application of high spatial resolution satellite imagery for riparian and forest ecosystem classification. *Remote Sens. Environ.* **2007**, *110*, 29–44. [[CrossRef](#)]
- Pu, R.; Landry, S. A comparative analysis of high spatial resolution IKONOS and WorldView-2 imagery for mapping urban tree species. *Remote Sens. Environ.* **2012**, *124*, 516–533. [[CrossRef](#)]
- Reiche, J.; Mullissa, A.; Slagter, B.; Gou, Y.; Tsendbazar, N.-E.; Odongo-Braun, C.; Vollrath, A.; Weisse, M.J.; Stolle, F.; Pickens, A.; et al. Forest disturbance alerts for the Congo Basin using Sentinel-1. *Environ. Res. Lett.* **2021**, *16*, 024005. [[CrossRef](#)]
- Korhonen, L.; Hadi; Packalen, P.; Rautiainen, M. Comparison of Sentinel-2 and Landsat 8 in the estimation of boreal forest canopy cover and leaf area index. *Remote Sens. Environ.* **2017**, *195*, 259–274. [[CrossRef](#)]

27. Ganz, S.; Adler, P.; Kändler, G. Forest Cover Mapping Based on a Combination of Aerial Images and Sentinel-2 Satellite Data Compared to National Forest Inventory Data. *Forests* **2020**, *11*, 1322. [[CrossRef](#)]
28. Zhang, Y.; Ling, F.; Wang, X.; Foody, G.M.; Boyd, D.S.; Li, X.; Du, Y.; Atkinson, P.M. Tracking small-scale tropical forest disturbances: Fusing the Landsat and Sentinel-2 data record. *Remote Sens. Environ.* **2021**, *261*, 112470. [[CrossRef](#)]
29. Lima, T.A.; Beuchle, R.; Langner, A.; Grecchi, R.C.; Griess, V.C.; Achard, F. Comparing Sentinel-2 MSI and Landsat 8 OLI Imagery for Monitoring Selective Logging in the Brazilian Amazon. *Remote Sens.* **2019**, *11*, 961. [[CrossRef](#)]
30. Bullock, E.L.; Healey, S.P.; Yang, Z.; Houborg, R.; Gorelick, N.; Tang, X.; Andrianirina, C. Timeliness in forest change monitoring: A new assessment framework demonstrated using Sentinel-1 and a continuous change detection algorithm. *Remote Sens. Environ.* **2022**, *276*, 113043. [[CrossRef](#)]
31. Zanaga, D.; Van De Kerchove, R.; De Keersmaecker, W.; Souverijns, N.; Brockmann, C.; Quast, R.; Wevers, J.; Grosu, A.; Paccini, A.; Vergnaud, S.; et al. ESA WorldCover 10 m 2020 v100. Available online: <https://doi.org/10.5281/zenodo.5571936> (accessed on 20 October 2021).
32. Jia, K.; Liang, S.; Zhang, L.; Wei, X.; Yao, Y.; Xie, X. Forest cover classification using Landsat ETM+ data and time series MODIS NDVI data. *Int. J. Appl. Earth Obs. Geoinf.* **2014**, *33*, 32–38. [[CrossRef](#)]
33. Alonso, L.; Picos, J.; Armesto, J. Forest Land Cover Mapping at a Regional Scale Using Multi-Temporal Sentinel-2 Imagery and RF Models. *Remote Sens.* **2021**, *13*, 2237. [[CrossRef](#)]
34. Brown, C.F.; Brumby, S.P.; Guzder-Williams, B.; Birch, T.; Hyde, S.B.; Mazzariello, J.; Czerwinski, W.; Pasquarella, V.J.; Haertel, R.; Ilyushchenko, S.; et al. Dynamic World, Near real-time global 10 m land use land cover mapping. *Sci. Data* **2022**, *9*, 251. [[CrossRef](#)]
35. Qi, W.; Li, H.; Zhang, Q.; Zhang, K. Forest restoration efforts drive changes in land-use/land-cover and water-related ecosystem services in China's Han River basin. *Ecol. Eng.* **2019**, *126*, 64–73. [[CrossRef](#)]
36. Potapov, P.; Li, X.; Hernandez-Serna, A.; Tyukavina, A.; Hansen, M.C.; Kommareddy, A.; Pickens, A.; Turubanova, S.; Tang, H.; Silva, C.E.; et al. Mapping global forest canopy height through integration of GEDI and Landsat data. *Remote Sens. Environ.* **2021**, *253*, 112165. [[CrossRef](#)]
37. Sexton, J.O.; Song, X.-P.; Feng, M.; Noojipady, P.; Anand, A.; Huang, C.; Kim, D.-H.; Collins, K.M.; Channan, S.; DiMiceli, C.; et al. Global, 30-m resolution continuous fields of tree cover: Landsat-based rescaling of MODIS vegetation continuous fields with lidar-based estimates of error. *Int. J. Digital Earth* **2013**, *6*, 427–448. [[CrossRef](#)]
38. Du, Z.; Yu, L.; Yang, J.; Coomes, D.; Kanniah, K.; Fu, H.; Gong, P. Mapping Annual Global Forest Gain From 1983 to 2021 with Landsat Imagery. *IEEE J. Sel. Top. Appl. Earth Obs. Remote Sens.* **2023**, *16*, 4195–4204. [[CrossRef](#)]
39. Guo, J.; Gong, P.; Dronova, I.; Zhu, Z. Forest cover change in China from 2000 to 2016. *Int. J. Remote Sens.* **2022**, *43*, 593–606. [[CrossRef](#)]
40. Stehman, S.V. Sampling designs for accuracy assessment of land cover. *Int. J. Remote Sens.* **2009**, *30*, 5243–5272. [[CrossRef](#)]
41. Stehman, S.V. Estimating area and map accuracy for stratified random sampling when the strata are different from the map classes. *Int. J. Remote Sens.* **2014**, *35*, 4923–4939. [[CrossRef](#)]
42. Steinhausen, M.J.; Wagner, P.D.; Narasimhan, B.; Waske, B. Combining Sentinel-1 and Sentinel-2 data for improved land use and land cover mapping of monsoon regions. *Int. J. Appl. Earth Obs. Geoinf.* **2018**, *73*, 595–604. [[CrossRef](#)]
43. Zhang, W.; Brandt, M.; Wang, Q.; Prishchepov, A.V.; Tucker, C.J.; Li, Y.; Lyu, H.; Fensholt, R. From woody cover to woody canopies: How Sentinel-1 and Sentinel-2 data advance the mapping of woody plants in savannas. *Remote Sens. Environ.* **2019**, *234*, 111465. [[CrossRef](#)]
44. Nasiri, V.; Sadeghi, S.M.; Moradi, F.; Afshari, S.; Deljouei, A.; Griess, V.C.; Maftei, C.; Borz, S.A. The Influence of Data Density and Integration on Forest Canopy Cover Mapping Using Sentinel-1 and Sentinel-2 Time Series in Mediterranean Oak Forests. *ISPRS Int. J. Geo-Inf.* **2022**, *11*, 423. [[CrossRef](#)]
45. Yang, Y.; Wu, T.; Wang, S.; Li, J.; Muhanmmad, F. The NDVI-CV Method for Mapping Evergreen Trees in Complex Urban Areas Using Reconstructed Landsat 8 Time-Series Data. *Forests* **2019**, *10*, 139. [[CrossRef](#)]
46. Chen, J.; Jönsson, P.; Tamura, M.; Gu, Z.; Matsushita, B.; Eklundh, L. A simple method for reconstructing a high-quality NDVI time-series data set based on the Savitzky–Golay filter. *Remote Sens. Environ.* **2004**, *91*, 332–344. [[CrossRef](#)]
47. Feng, G.; Masek, J.; Schwaller, M.; Hall, F. On the blending of the Landsat and MODIS surface reflectance: Predicting daily Landsat surface reflectance. *IEEE Trans. Geosci. Remote Sens.* **2006**, *44*, 2207–2218. [[CrossRef](#)]
48. Zhu, X.; Chen, J.; Gao, F.; Chen, X.; Masek, J.G. An enhanced spatial and temporal adaptive reflectance fusion model for complex heterogeneous regions. *Remote Sens. Environ.* **2010**, *114*, 2610–2623. [[CrossRef](#)]
49. Li, X.; Foody, G.M.; Boyd, D.S.; Ge, Y.; Zhang, Y.; Du, Y.; Ling, F. SFSDAF: An enhanced FSDAF that incorporates sub-pixel class fraction change information for spatio-temporal image fusion. *Remote Sens. Environ.* **2020**, *237*, 111537. [[CrossRef](#)]

**Disclaimer/Publisher's Note:** The statements, opinions and data contained in all publications are solely those of the individual author(s) and contributor(s) and not of MDPI and/or the editor(s). MDPI and/or the editor(s) disclaim responsibility for any injury to people or property resulting from any ideas, methods, instructions or products referred to in the content.